Noncanonical TRAIL Signaling Facilitates Tumor Immunosuppression and Cholangiocarcinoma Growth via Myeloid-Derived Suppressor Cells

Emilien Loeuillard[1], Binbin Li[1], Hannah E. Stumpf[1], Jingchun Yang[1], Jennifer L. Tomlinson[2], Rondell P. Graham[3], Rory L. Smoot[2], Haidong Dong[4,5], Sumera I. Ilyas[1,4#]

[1]Division of Gastroenterology and Hepatology, Mayo Clinic, Rochester, MN, USA, [2]Department of Surgery, Mayo Clinic College of Medicine and Science, Rochester, MN, USA, [3]Department of Laboratory Medicine and Pathology, Mayo Clinic College of Medicine and Science, Rochester, MN, USA, [4]Department of Immunology, Mayo Clinic College of Medicine and Science, Rochester, MN, USA, [5]Department of Urology, Mayo Clinic College of Medicine and Science, Rochester, MN, USA

[#]Corresponding author: Sumera I. Ilyas, M.B.B.S.
Assistant Professor of Immunology and Medicine
Mayo Clinic College of Medicine and Science
200 First Street SW
Rochester, Minnesota 55905
Tel.: 507 538 4877; Fax: 507 284 0762

C**onflicts of Interest:** The authors declare no potential conflicts of interest.

Keywords: Cholangiocarcinoma, immune evasion, granulocytic-MDSCs, NF-κB.

Abbreviations: CCA, cholangiocarcinoma; CTL, cytotoxic T lymphocyte; G-MDSCs, granulocytic-MDSCs; ICI, immune checkpoint inhibition; MDSCs, myeloid-derived suppressor cells; M-MDSCs, monocytic-MDSCs; PD-1, programmed death-1; PD-L1, programmed death-ligand 1; TRAIL, Tumor necrosis factor related apoptosis inducing ligand; TIME, tumor immune microenvironment.

ABSTRACT

Proapoptotic tumor necrosis factor related apoptosis inducing ligand (TRAIL) signaling as a cause of cancer cell death is a well-established mechanism. However, TRAIL-receptor (TRAIL-R) agonists have had very limited anticancer activity in humans, challenging this concept of TRAIL as a potent anticancer agent. Herein, we demonstrate that TRAIL+ cancer cells can leverage non-canonical TRAIL signaling to foster myeloid-derived suppressor cell (MDSC) accumulation in murine cholangiocarcinoma (CCA). In multiple immunocompetent syngeneic, orthotopic murine models of CCA, implantation of TRAIL+ murine cancer cells into *Trail-r*$^{-/-}$ mice resulted in a significant reduction in tumor volumes compared to wild-type mice. Tumor bearing *Trail-r*$^{-/-}$ mice had a significant decrease in abundance of MDSCs. Accordingly, genetic deletion of *Trail-r* decreased murine tumor progression via a significant reduction in MDSCs due to attenuation of MDSC proliferation. Moreover, MDSCs were resistant to TRAIL-mediated apoptosis, and noncanonical TRAIL signaling activated NF-κB signaling in MDSCs. Finally, cancer cell restricted deletion of *Trail* significantly reduces tumor burden. In summary, our findings highlight the therapeutic potential of targeting TRAIL+ cancer cells for the treatment of a poorly immunogenic cancer.

INTRODUCTION

Tumor necrosis factor related apoptosis inducing ligand (TRAIL), a member of the tumor necrosis factor super family, is predominantly expressed on immune cells, which use it as an important mechanism to induce cancer cell death by apoptosis.[1] Two TRAIL receptors are expressed in humans, TRAIL-receptor 1 or death receptor 4 (TRAIL-R1/DR4, TNFRSF10A) and TRAIL-R2 (DR5, TNFRSF10B).[2,3] Mice only have a single TRAIL receptor (death receptor 5 [Dr5]; Trail-r).[4] The TRAIL-TRAIL-R system has garnered considerable interest in cancer biology, especially as a potential anti-cancer therapy.[1] In multiple murine models of tumorigenesis, *Trail* deficiency renders mice more susceptible to carcinogenesis and tumor progression.[1] In addition to triggering cancer cell apoptosis, TRAIL-TRAIL-R system has various effects on the tumor immune microenvironment (TIME) including reduction in the abundance of pro-tumor myeloid cells as well as activation of CTLs and natural killer (NK) cells.[1,5-7] However, TRAIL-R agonists have had very limited anti-cancer activity in humans,[1] challenging this concept of TRAIL as an anti-cancer agent. Indeed, emerging information suggests that TRAIL may have a protumor role as it can foster tumor proliferation as well as invasion.[8-11] Hence, in addition to having a tumor suppressive role, TRAIL may act as a pro-tumor cytokine that fosters tumor growth and progression.

The effect of TRAIL-TRAIL-R on the TIME is not well-defined; limited evidence suggests that the influence of TRAIL-TRAIL-R on the TIME is multifaceted and context dependent. In certain malignancies such as thymoma and breast cancer, TRAIL-TRAIL-R reduces abundance of myeloid-derived suppressor cells (MDSC) by promoting MDSC apoptosis.[6,7] In contrast, TRAIL induces a pro-myeloid secretome in lung adenocarcinoma.[8] Thus, the potency and hierarchy of TRAIL anti-cancer versus pro-cancer processes in cancer biology has yet to be defined.

TRAIL ligation of its cognate receptors induces activation of pro-apoptotic signaling pathways, and triggers the extrinsic pathway of cellular apoptosis.[12] Non-apoptotic signaling cascades promoting pro-inflammatory gene transcription programs and activation of NF-κB have also been described.[13]

However, the biology and pathobiology of non-canonical TRAIL mediated signaling in cancer immunology has not been well-defined.

Cholangiocarcinoma (CCA) is a desmoplastic cancer originating from the bile ducts.[14] Immunotherapeutic approaches have had subpar impact on patient survival with low response rates in highly lethal cancers such as CCA. Indeed, the results with ICI monotherapy in 'immune cold' tumors such as CCA and pancreatic ductal adenocarcinoma (PDAC) have been disappointing with an overall response rate of <10%,[15,16] implying that tumor cells ultimately evade the anti-tumor immune response and further anticancer immune stimulation is necessary. We have demonstrated that the CCA TIME is poorly immunogenic with an abundance of pro-tumor myeloid cells such as tumor-associated macrophages (TAMs) and myeloid-derived suppressor cells (MDSCs) and a paucity of CTLs in the tumor core.[17] MDSCs are a heterogeneous group of immature myeloid cells that promote immune tolerance, mediate tumor immune escape and immunotherapy resistance with consequent tumor progression.[18] MDSC subsets include monocytic MDSCs (M-MDSC) that are $CD11b^{+}Ly6G^{-}Ly6C^{high}$ and granulocytic MDSCs (G-MDSC) that are $CD11b^{+}Ly6G^{+}Ly6C^{low}$.[18-23] We have demonstrated that therapeutic targeting of TAMs did not reduce cholangiocarcinoma (CCA) tumor burden in mice due to a compensatory emergence of MDSCs, highlighting the integral role of MDSCs in the CCA TIME.[17]

It is unknown whether non-canonical TRAIL signaling can increase survival and proliferation of MDSCs. Herein, we examine the role of TRAIL biology in CCA by employing unique immunocompetent murine models. The TRAIL-TRAIL-R system has a dual role in the CCA tumor immune microenvironment by facilitating cancer cell apoptosis (canonical) while promoting an immunosuppressive tumor microenvironment by directly fostering MDSC abundance and function (non-canonical).

RESULTS

TRAIL-R^{+} immune cells in the TIME are essential in facilitating tumor progression.

Whereas TRAIL receptors are ubiquitously expressed, TRAIL is predominantly expressed on cells of the immune system which use it as an important mechanism to induce cancer cell death by apoptosis.[1] Using

single cell RNA sequencing (scRNA seq) of human CCA tumors, we demonstrated that CCA cells also express *TNFSF10* whereas immune cells express *TNFRSF10A* and *TNFRSF10B* in human CCA **(Fig. 1A-B)**. Accordingly, the TRAIL-TRAIL-R system may have pleiotropic effects on the CCA TIME.

To further examine the role of the TRAIL-TRAIL-R system in the CCA TIME, we leveraged our unique murine models of CCA that distinct genetic drivers and are an optimal tool for assessing the influence of TRAIL-TRAIL-R on the TIME. Murine CCA cells (SB, FAC, KPPC) have constitutive or cell autonomous TRAIL expression as there is abundant TRAIL protein expression in vitro in these cells despite isolation from the liver (**Supplementary Fig. S1A)**. Murine CCA cells were implanted into livers of C57BL/6J and *Trail-r*$^{-/-}$ mice. Hence, in this model the host immune cells express TRAIL but not the receptor and would be capable of inducing TRAIL-mediated apoptosis in CCA cells but would be resistant to potential TRAIL-mediated immunosuppression **(Fig. 1C)**. Implantation of SB cells into *Trail-r*$^{-/-}$ mice results in a significant reduction in tumor volumes compared to WT mice **(Fig. 1C-E; Supplementary Fig. S1B)**. Similarly, a significant reduction in tumor volumes was noted in *Trail-r*$^{-/-}$ mice compared to WT mice using the KPPC model **(Fig. 1F-H; Supplementary Fig. S1C)**. Tumors were also reduced in FAC tumor bearing *Trail-r*$^{-/-}$ mice compared to WT mice (**Fig. 1I-K)**. Taken together, these results suggest that TRAIL-R^{+} host immune cells are essential in facilitating tumor progression.

Genetic deletion of *Trail-r* augments CTL infiltration and function

Tumors arising in mice genetically deficient in *Trail-r* exhibited enhanced CD8^{+} T cell infiltration compared to WT SB and KPPC mice tumors **(Fig. 2A-B; Supplementary Fig. S2A)**. Reactive CTLs express CD11a, an integrin, which is upregulated in effector and memory CD8^{+} T cells. CD11a mediates conjugation between CTLs and target cells and can be used to identify and monitor endogenous tumor-reactive CTLs.[24,25] *Trail-r*$^{-/-}$ tumors had a significant increase in tumor-reactive CD8^{+} T cells and had enhanced CTL effector function **(Fig. 2C-E)**. There was no significant difference in the abundance of CD4^{+} T cells in *Trail-r*$^{-/-}$ tumors compared to WT tumors, albeit there was a significant reduction in NK cells in *Trail-r*$^{-/-}$ tumors (**Supplementary Fig. S2B, S2C)**. The TRAIL-TRAIL-R system has been implicated in T cell homeostasis.[26] Although we postulated that TRAIL-TRAIL-R may directly impact

CTL apoptosis or proliferation, we did not observe an increase in CTL apoptosis albeit an increase in proliferation was noted in *Trail-r*$^{-/-}$ tumors **(Fig. 2F, 2G)**. To further examine this, murine T cells were isolated from WT or *Trail-r*$^{-/-}$ mice and cocultured with CCA (SB) cells **(Fig. 2H)**. No difference in T cell proliferation or apoptosis was noted between WT-CD8^{+} T cells and *Trail-r*$^{-/-}$ -CD8^{+} T cells when cocultured with murine CCA cells, indicating that TRAIL-TRAIL-R does not have a direct effect on T cell proliferation or apoptosis **(Fig. 2I)**. Moreover, in the presence of murine SB cells, WT CD8^{+} T cells had no change in markers of activation, effector function, or exhaustion when compared to *Trail-r*$^{-/-}$ CD8^{+} T cells **(Supplementary Fig. S2D-2G)**. Finally, to definitely determine whether TRAIL-TRAIL-R has a direct impact on CD8^{+} T cells, we generated mice with CD8^{+} T cell specific knockout of the *Trail-r* gene by crossing a mouse floxed for the *Trail-r* gene with a Cd8a-cre mouse, a transgenic mouse with Cre activity noted in peripheral CD8^{+} T cells.[27] SB cells were implanted orthotopically into livers of *Trail-r*$^{f/f}$ and Cd8^{cre-}*Trail-r*$^{f/f}$ mice (ΔCd8) **(Fig. 2J)**. There was a significant reduction in SB tumor weight in Cd8^{cre-}*Trail-r*$^{f/f}$ mice compared with *Trail-r*$^{f/f}$ mice **(Fig. 2K and E)**. These data suggest that TRAIL-TRAIL-R does not have a direct effect on CD8+ T cells, and the increased CTL abundance in *Trail-r*$^{-/-}$ mice be an indirect effect in the CCA TIME via modulation of immunosuppressive cells by TRAIL-TRAIL-R.

Genetic deletion of *Trail-r* restricts murine tumor progression via a significant reduction in MDSCs.

As TRAIL signaling did not appear to have a direct suppressive effect on cytotoxic elements within the CCA TIME, we next examined the immunosuppressive cell types. *Trail-r*$^{-/-}$ tumors exhibited a significant reduction in MDSCs and macrophages **(Fig. 3A; Supplementary Fig. S3A-B)**, while there was no difference in the abundance of dendritic cells (**Supplementary Fig. S3C)**. *Trail-r*$^{-/-}$ SB tumors had a significant attenuation of CD11b^{+}Ly6G^{+}Ly6C^{-} G-MDSCs without a significant alteration of CD11b^{+}Ly6G^{-}Ly6C^{+} M-MDSCs **(Fig. 3A)**. *Trail-r*$^{-/-}$ SB tumors also had a significant decrease in CD11b^{+}F4/80^{+} macrophages compared to WT SB tumors. CD206^{+} TAMs were decreased in *Trail-r*$^{-/-}$ SB tumors, whereas M1-like macrophages, which are typically anti-tumor, pro-inflammatory, were

significantly increased **(Supplementary Fig. S3A and S3B)**. These data support the notion that *Trail-r*$^{-/-}$ SB tumors have a pro-inflammatory, anti-tumor milieu which contributes to a significant reduction in tumor volumes in the context of genetic *Trail-r* deficiency. In comparison, *Trail-r*$^{-/-}$ KPPC tumors had a significant decrease in M-MDSCs rather than G-MDSCs **(Fig. 3B).** Additionally, *Trail-r*$^{-/-}$ KPPC tumors had no significant change in macrophages (**Supplementary Fig. S3D and S3E)**, which is consistent with our prior observation that SB and KPPC tumors have distinct immune microenvironments, yet both models demonstrated a significant decrease in MDSCs in the context of *Trail* deficiency.

As we have previously demonstrated that MDSCs and TAMs play an integral role in the progression of CCA,[17] we postulated that TRAIL-TRAIL-R promotes tumor progression by mediating tumor immune evasion via these immunosuppressive myeloid cells. To further examine this concept, we employed myeloid cell restricted deletion of *Trail-r*. To determine the impact of *Trail-r* deficiency in MDSCs and macrophages, we generated mice with myeloid cell specific knockout of the *Trail-r* gene by crossing a mouse floxed for the *Trail-r* gene with a LysM-cre mouse.[28] SB cells were implanted orthotopically into livers of *Trail-r* $^{f/f}$ and LyzM^{cre-}*Trail-r*$^{f/f}$ mice (Δmye) **(Fig. 3C)**. There was a significant reduction in SB tumor weight in LyzM^{cre-}*Trail-r* $^{f/f}$ mice compared with *Trail-r* $^{f/f}$ mice **(Fig. 3D and E)**. Similar to our observations in *Trail-r*$^{-/-}$ SB tumors, LyzM^{cre-}*Trail-r* $^{f/f}$ SB tumors had a significant increase in CD8^{+} T cell and tumor-reactive CD8^{+} T cells compared to *Trail-r* $^{f/f}$ SB tumors **(Fig. 3F)**. Consistently, G-MDSCs were also significantly reduced in LyzM^{cre-}*Trail-r* $^{f/f}$ SB tumors while no change was observed in M-MDSCs **(Fig. 3G and H)**. In contrast to *Trail-r*$^{-/-}$ SB tumors, myeloid cell restricted deletion of *Trail-r* did not influence macrophage abundance, suggesting that MDSCs are the cell type primarily impacted by TRAIL-TRAIL-R (**Supplementary Fig. S3F and S3G)**. In aggregate, these observations confirm that TRAIL-TRAIL-R promotes tumor progression by decreasing tumor infiltrating CTLs, likely via augmentation of MDSC abundance.

TRAIL-TRAIL-R augments MDSCs abundance via enhanced proliferation

Next, we sought to clarify whether TRAIL-TRAIL-R has a direct effect on MDSC abundance via enhanced proliferation or attenuation of apoptosis. G-MDSCs in *Trail-r*$^{-/-}$ tumors had no change in

apoptosis compared to MDSCs in WT mouse tumors, suggesting that these cells are resistant to TRAIL-mediated apoptosis **(Fig. 4A)**. G-MDSCs in *Trail-r*$^{-/-}$ tumors did exhibit a significant suppression of proliferation, as assessed by Ki67, compared to MDSCs from WT SB tumors **(Fig. 4B)**. These findings were confirmed in tumor bearing LyzM^{cre-}*Trail-r*$^{f/f}$ mice; G-MDSCs had a significant suppression of proliferation without a change in apoptosis in the context of myeloid restricted deletion of *Trail-r* **(Fig. 4C-D)**. M-MDSC abundance is not altered in *Trail-r*$^{-/-}$ SB tumors **(Fig. 3A)**. Accordingly, no change was noted in apoptosis or proliferation of M-MDSCs in *Trail-r*$^{-/-}$ SB tumors or LysM^{cre-}*Trail-r* $^{f/f}$ SB tumors **(Supplementary Fig. S4A-B)**. Additionally, the percentage of arginase 1 or IL-10 expressing G-MDSCs or M-MDSCs was similar between WT, *Trail-r*$^{-/-}$, and LysM^{cre-}*Trail-r* $^{f/f}$ tumors **(Supplementary Fig. S4C-S4G)**. Overall, these results suggest that TRAIL signaling augments G-MDSC abundance in SB tumors via enhanced proliferation and M-MDSC abundance in KPPC tumors due to decreased apoptosis.

To determine whether enhanced MDSC proliferation is a direct effect of TRAIL signaling activation, we differentiated CD11b^{+}Ly6C^{+} MDSCs from bone marrow (BM) of WT and *Trail-r*$^{-/-}$ mice using growth factors as previously described.[29] We confirmed that WT BM-derived MDSCs express TRAIL-R **(Fig. 4E)**. WT and *Trail-r*$^{-/-}$ MDSCs were cocultured with murine tumor cells (SB cells) that express TRAIL protein (**Supplementary Fig. S1A)** and MDSCs were subsequently harvested for further analysis via flow cytometry **(Fig. 4E)**. MDSCs from *Trail-r*$^{-/-}$ mice (*Trail-r*$^{-/-}$-MDSCs) had a significant decrease in proliferation compared to MDSCs from WT mice (WT MDSCs) when cocultured with tumor cells **(Fig. 4F),** suggesting that TRAIL^{+} cancer cells bind to TRAIL-R on MDSCs and directly influence MDSC abundance by increasing MDSC proliferation. Collectively, these data demonstrate that TRAIL-TRAIL-R directly influences MDSC abundance by increasing MDSC proliferation, and G-MDSCs are resistant to TRAIL-mediated apoptosis in murine CCA tumors.

Non-canonical TRAIL-R signaling promotes MDSC survival in an NF-κB dependant manner.

Activation of the classical NF-κB pathway leads to phosphorylation and degradation of inhibitor of κB (IκB) kinase complex which liberates NF-κB dimers with subsequent nuclear translocation of NF-κB subunits p50 and p65.[30] We have observed that MDSCs are resistant to TRAIL-mediated apoptosis

while TRAIL signaling augments MDSC proliferation **(Fig. 4A-B)**. To delineate whether this observed effect of TRAIL signaling on MDSC proliferation is occurring via non-canonical TRAIL signaling, we examined NF-kB activation in WT MDSCs and *Trail-r*$^{-/-}$-MDSCs incubated with murine SB cells. *Trail-r*$^{-/-}$-MDSC had a significant increase in the nuclear translocation of p65 (**Fig. 5A**) compared to WT MDSCs when co-cultured with tumor cells, suggesting that TRAIL-TRAIL-R may augment MDSC proliferation via NF-kB. Next, we examined the impact of NF-kB signaling inhibition using a small molecule inhibitor of IKKα/β, TPCA-1,[31] on murine MDSC proliferation. TPCA-1 significantly reduced proliferation of WT MDSCs cocultured with SB cells (**Fig. 5B-C**). TPCA also reduced nuclear translocation of NF-κB of WT MDSCs cocultured with SB cells (**Fig. Supplementary Fig. S5A**). We then conducted single cell RNA sequencing of CD45^{+} cells isolated from murine SB, KPPC, and FAC tumors. Unsupervised clustering revealed 11 clusters of immune cells in the murine tumors. A significant enrichment of a previously reported NF-kB activation signature[32] was noted in the G-MDSC cluster. Collectively, these data indicate that non-canonical TRAIL signaling will result in increased NF-kB activation in MDSCs with consequent enhanced proliferation.

Cancer cell restricted deletion of *Trail* significantly reduces tumor burden.

Our data suggest that TRAIL^{+} cancer cells can leverage TRAIL signaling to evade the anti-tumor immune response. To determine whether targeting TRAIL+ cancer cells has therapeutic potential, we employed cancer cell restricted deletion by generating SB cells with CRISPR-Cas9-mediated knockdown of *Trail* (SB-*Trail*$^{-/-}$) **(Fig. 6A)**. We also generated SB-*Trail-r*$^{-/-}$. Implantation of SB-*Trail*$^{-/-}$ into WT C57BL/6J mice resulted in a significant reduction in the tumor burden compared to control SB cell (SB-non-targeting [NT]) implantation **(Fig. 6B-C; Supplementary Fig. S6A)**. Concordant with this and similar to our findings in the SB tumor bearing *Trail*$^{-/-}$ mice, there was a significant decrease in G-MDSCs in the SB-*Trail*$^{-/-}$ tumors without a change in M-MDSCs or macrophages **(Fig. 6D-E; Supplementary Fig. S6B-D)**. Moreover, CTLs and reactive CTLs were also significantly increased in SB-*Trail*$^{-/-}$ tumors **(Fig. 6F-G)**. To confirm that the alteration in MDSC abundance is related to TRAIL-mediated augmentation of MDSC proliferation, CD11b^{+}Ly6C^{+} MDSCs were differentiated from BM of WT mice

and cocultured with SB-NT and SB-*Trail*$^{-/-}$ cells **(Fig. 6H)**. Consistently, we demonstrated that in the presence of cancer cells devoid of *Trail*, MDSC proliferation was significantly suppressed, while MDSC apoptosis or markers of immunosuppression were unchanged **(Fig. 6I)**. These results suggest that cancer cell restricted deletion of *Trail* hinders tumor growth as Trail^{+} cancer cells cannot trigger a TRAIL-R mediated increase in MDSC abundance. Interestingly, SB-*Trail-r*$^{-/-}$ cell implantation into WT mice resulted in larger tumors compared to control **(Fig. 6B-C; Supplementary Fig. S6A)**. Consistent with existing knowledge, these results indicate that cancer cell restricted deletion of *Trail-r* has a tumor promoting effect as Trail^{+} cytotoxic immune cells cannot trigger TRAIL-R mediated cancer cell apoptosis. In aggregate, these data suggest that TRAIL-TRAIL-R has divergent roles in the tumor immune microenvironment (TIME): TRAIL+ cytotoxic immune cells can trigger cancer cell death, whereas TRAIL+ cancer cells can leverage non-canonical TRAIL signaling to evade the anti-tumor immune response. However, the pro-tumor, immunosuppressive role of TRAIL-TRAIL-R is more potent given that *Trail-r*$^{-/-}$ mice have a significant reduction in tumor burden.

Finally, to ascertain the human relevance of our findings, we interrogated a gene-expression dataset derived from patients with CCA (GSE76297). Using a previously published MDSC gene signature,[17,33] we observed that patients with higher levels of *TRAIL* had significantly higher MDSC gene expression compared to those with lower MDSC gene expression. These results are consistent with our preclinical observations that TRAIL augments MDSC abundance.

DISCUSSION

We have identified a potent immunosuppressive role of TRAIL signaling in the CCA TIME. These data indicate that (a) TRAIL-TRAIL-R actively supports tumor growth as *Trail-r* deficiency across multiple immunocompetent models of CCA significantly reduces tumor volumes; (b) TRAIL signaling promotes MDSC accumulation in murine CCA tumors; (c) MDSCs are resistant to TRAIL-mediated apoptosis; (d) noncanonical TRAIL signaling augments MDSC abundance via enhanced proliferation in an NF-κB dependent manner; (e) cancer cell restricted deletion of *Trail* significantly reduces tumor burden via a decrease in MDSC abundance.

Pro-apoptotic TRAIL signaling as a cause of cancer cell death is a well-established mechanism, whereby TRAIL^{+} cytotoxic immune cells such as NK cells bind to TRAIL-R on cancer cells with consequent cancer cell apoptosis. However, TRAIL-R agonists have had very limited anti-cancer activity in human clinical trials. The existing literature indicates that the effects of TRAIL signaling in the TIME are pleiotropic and context dependent. Whole body *Trail-r* deficiency in several murine models of tumorigenesis (e.g., breast cancer, renal cell carcinoma) renders mice more susceptible to primary tumor growth and metastasis. In contrast, TRAIL induced cytokine secretion from TRAIL-resistant cancer cells promotes a tumor supportive TIME in lung adenocarcinoma. This TRAIL-triggered secretome promotes MDSCs and M2-like macrophages, indicating a tumor promoting immune modulatory role of TRAIL signaling. Similarly, our data has demonstrated a significant reduction in CCA tumor burden of *Trail-r* deficient mice. However, the TRAIL secretome described in lung adenocarcinoma[8] is intact in our model as the CCA cells implanted into mouse livers express both *Trail* and *Trail-r* while the immune cells lack *Trail-r*, suggesting an alternate mechanism for TRAIL induced increase in MDSCs in the CCA TIME.

Noncanonical TRAIL signaling cascades can predominate in certain contexts, promoting proinflammatory gene transcription programs and activation of NF-κB,[13,34] but the role of noncanonical TRAIL signaling in tumor immunology is not clear.[1,26,35] In cells that are resistant to TRAIL-induced apoptosis, NF-κB activation via non-canonical TRAIL signaling can induce proliferation.[34] For instance, TRAIL signaling can induce proliferation of TRAIL-resistant tumor cells in an NF-κB dependent manner.[9,34] Our study has found that this paradigm also exists in MDSCs as WT MDSCs had NF-κB activation that was abrogated in *Trail-r*$^{-/-}$-MDSCs, and NF-κB inhibition attenuated TRAIL-mediated increase in MDSC proliferation. Moreover, single cell transcriptomics demonstrated that MDSCs across multiple murine models had significant enrichment of an NF-κB activation signature.

The combination of immunotherapeutics (e.g., ICI) and TRAIL-targeting therapies has been assessed in preclinical models of cancer.[36-39] However, these combinatorial approaches have employed TRAIL agonism, rather than selective TRAIL antagonism on cancer cells. We have now demonstrated that cancer cell restricted deletion of *Trail* significantly reduced MDSC accumulation with a consequent

reduction in tumor burden. Conversely, cancer cell restricted deletion of *Trail-r* increased murine tumor growth by promoting MDSC abundance and function. These observations highlight that systemic inhibition of TRAIL-TRAIL-R may lead to unwanted attenuation of apoptosis of TRAIL-R$^+$ CCA cells by TRAIL$^+$ immune cells. In summary, our findings support the role of selective therapeutic targeting of TRAIL$^+$ cancer cells in an effort to block TRAIL-TRAIL-R mediated tumor immunosuppression.

METHODS

Mice

All animal experiments were performed in accordance with a protocol approved by the Mayo Clinic Institutional Animal Care and Use Committee (IACUC). Eight-week-old male C57BL/6J mice, and LysM^{cre} C57BL/6J mice were purchased from Jackson Laboratories. *Trail-r*$^{f/f}$, *Trail*$^{f/f}$ and *Trail-r*$^{-/-}$ were bred at Mayo Clinic. LysM^{cre} mice are myeloid-cre expression mice with high recombination rates in myeloid cells including mature macrophage and MDSCs.[28]

Syngeneic, orthotopic murine models of CCA

We have established multiple, syngeneic immunocompetent models of CCA that recapitulate human CCA and have distinct genetic drivers.[40-42] The SB murine CCA cell line and the resultant syngeneic model are derived from a genetic model employing biliary instillation of the oncogenes Akt and yes-associated protein (YAP^{S127A}).[40] This Akt/YAP driven model has substantial overlap with human iCCA.[40] Mutations inducing activation of the oncogene *Kras* and inactivation of the tumor suppressor gene *p53* are common genetic alteration in CCA.[43,44] *Kras*^{G12D}*p53*$^{L/L}$ murine CCA tumors (KPPC) are more aggressive than SB tumors and have a distinct phenotype representing a sarcomatoid CCA subtype, a rare and aggressive subtype of human iCCA driven by *Kras*^{G12D}*p53*$^{L/L}$.[45] In contrast, implantation of CCA cells (FAC) derived from a genetic model driven by loss of FBXW7 and permissive Akt[46], results in a syngeneic model with slower tumor growth than the SB model (manuscript submitted). Murine CCA cells (SB, KPPC, FAC)[40,42,46] were maintained in culture medium as previously described.[41] Mice were anesthetized and 20 µL of standard media containing 0.75 x 10^6 SB, KPPC, or FAC cells were injected orthotopically into the lateral aspect of the medial lobe as previously described.[17,41] Mice were sacrificed two, four, and five weeks after implantation of KPPC, SB, and FAC cells, respectively. Tumor, adjacent liver, and spleen were harvested following sacrifice.

Generation of SB *Trail*$^{-/-}$ and *Trail-r*$^{-/-}$ cells

CRISPR-Cas9-mediated knockout of mouse *Trail* and *Trail-r* in SB cells was conducted using the dual single guide RNA vector system pSpCas9(bb)-2A-GFP (PX458). The sgRNA sequences sgRNA1-Trail-r,

sgRNA2-Trail-r, forward-Trail-r, reverse-Trail-r, sgRNA1-Trail, sgRNA2-Trail, forward-Trail and reverse-Trail were generated in PZH vector amplified and extracted using In-Fusion HD Cloning kit (Clontech). Plasmids were sent for Sanger sequencing with reverse and forward primer to control any mutation point. SB cells were then transfected using lipofectamine 3000 transfection kit (Invitrogen). SB clone knockout for Trail or Trail-r were selected by PCR.

(Table 1)

sgRNA1-Trai-r	CTTGTGGAAAGGACGAAA CACC TCAGGCCAGTACCTGTCAGA GTTTTAGAGCTAGAAATAGC
sgRNA2-Trail-r	ACTTGCTATTTCTAGCTCTA AAAC TACAGACTGTGCAGAGAATA AGAGACGTCCGTCTCCGGT
Forward-Tral-r	CAGGCAGTCCCTCAGTTGTG
Reverse-Trail-r	AAAGACAGGCGGAGAACAGG
sgRNA1-Trail	CTTGTGGAAAGGACGAAA CACC GGAGTAATTGTCCTGCAGCT GTTTTAGAGCTAGAAATAGC
sgRNA2-Trail	ACTTGCTATTTCTAGCTCTA AAAC CTTAACCTGCAAGCAGGGTC AGAGACGTCCGTCTCCGGT
Forward-Trail	TAAACCACAAACTGCCCACG
Reverse-Trail	ACACCATATTGCTGGCGAAT

Isolation of liver, spleen, or tumor-infiltrating immune cells and flow analysis

Upon excision, tumor, and liver were dissociated with gentleMACS™ Octo Dissociator (Miltenyi) according to the manufacturer's protocol. $CD45^+$ cells were isolated by CD45 (TIL) mouse microbeads (Miltenyi). Cells were incubated with Fixable Viability Stain 510 (BD Horizon™) for 15 minutes followed by anti-Fc blocking reagent (Miltenyi) for 10 minutes prior to surface staining. Cells were stained, followed by data acquisition on a Miltenyi MACSQuant® Analyzer 10 optical bench flow cytometer. All antibodies were used following the manufacturer recommendation and Fluorescence Minus One controls were used for each independent experiment to establish gates. For subsequent intracellular staining of granzyme B, CD206, IL-10, Ki67 and Arginase1, cells were stained using the intracellular staining kit (Miltenyi). Apoptosis staining was performed using APC Annexin V apoptosis detection kit with 7-AAD (Biolegend). Analysis was performed using FlowJo™ (TreeStar). Forward scatter (FSC) and side scatter (SSC) were used to exclude cell debris and doublets.

Flow analysis antibodies

The following antibodies were used for flow cytometry staining: F4/80-PacificBlue (BM8, BioLegend®), CD11b-PE-Cy5 (M1/70, eBioscience™), CD11b-PE-Cy7 (M1/70, BioLegend®) CD206-

PE-Cy7 (C068C2, BioLegend®), CD11c-APC (REA754, Miltenyi), Gr-1-PE (RB6-8C5, BioLegend®), Ly6G-PE (REA526, Miltenyi), Ly6C-APC-Vio®770 (REA796, Miltenyi), Arginase1-PE-Cy7 (A1exF5, eBioscience™), IL-10-FITC (JES5-16E3, BioLegend®), Ki67-AF700 (16A8, BioLegend®), PD-L1-BV421 (10F.9G2, BioLegend®), CD3-APC-Cy7 (17A2, BioLegend®), CD8-BV421 (53-6.7, BD Horizon™), CD11a-PE-Vio®770 (REA880, Miltenyi), PD-1-PerCP-Vio®700 (REA802, Miltenyi), granzyme B-PE (QA16A02, BioLegend®), NK1.1-APC (PK136, Miltenyi), CD69-PE-Cy7 (H1.2F3, BioLegend®), TIM-3-FITC (REA602, Miltenyi), INFγ-PE (XMG1.2, BioLegend®) and 7AAD-annexinV-APC kit (640930, BioLegend®).

Isolation of Bone Marrow MDSC (BM-MDSC) and *in vitro* culture

BM-MDSCs were isolated from the leg of WT or *Trail-r*$^{-/-}$ mice. Bone marrow was extracted and filtered through 70um cell strainer. Single cell suspension was cultured in a MDSC medium activation (RPMI 1640 + 10% low endotoxin FBS + IL-6 40ng/ml + G-CSF 40ng/ml + GM-CSF 40ng/ml) for 5 days to induce MDSC differentiation. BM-MDSC were plated in 24-well plate at 1 x 10 ^{5} cell and co-cultured with SB cells at a 1:4 ratio or treated with TPCA 10µM for 24h. BM-MDSC were stained with Fixable Viability Stain 510 (BD Horizon™), CD11b-PE-Cy5, Gr-1-PE, PD-L1-BV421, IL-10-FITC, Arginase1-PE-Cy7, Ki67-AF700, AnnexinV-APC, 7-AAD and analyzed by flow cytometry. For Immunofluorescence, BM-MDSC were plated in 4 chamber culture slide at 7.5 x 10^{5} cells and co-cultured with SB cells at a ratio of 1:4 or treated with TPCA at 10µM for 24h. Cells were fixed with 4% paraformaldehyde, permeabilized with 0.1% Triton-x100 and incubated with conjugated antibodies CD45-AF594 (D3F8Q, Cell signaling, 1:50), NF-κB p65-AF647 (D14E12, Cell signaling 1:50) and Pan-CK-AF488 (C11, Cell signaling, 1:100) at 4°C overnight. Immunofluorescence was visualized on a Zeiss LSM980 confocal laser scanning microscope (Carl Zeiss Microscopy, LLC, White Plains, NY) using a 60X, 1.2 numerical aperture (NA) oil-immersion objective lens. Image analyses were done using Zen 3.4 (blue edition, Carl Zeiss Microscopy, LLC, White Plains, NY). For the SB conditioned medium BM-MDSC were incubated with SB cell conditioned medium for 0, 0.5, 1, 2 or 4h. BM-MDSC cytoplasmic and nuclear proteins were collected and NF-κB analyzed by western blot.

Isolation of T cells

$CD8^+$ T cells were isolated from a single cell suspension of WT or *Trail-r*$^{-/-}$ mouse spleens. Single cell suspension was filtered through 70µm mesh, centrifuged at 400 g for 10 minutes and re-suspended at $1x10^8$ cell/mL. $CD8^+$ T cells were isolated using easy step mouse $CD8^+$ T cell isolation kit (#19856, stemcell) per the manufacturer's protocol.

Immunoblot Analysis

Proteins were resolved by SDS-PAGE and transferred to nitrocellulose membranes. The following primary antibodies were used for immunoblotting analysis: polyclonal TRAIL (ABclonal) and NF-κB p65 (D14E12, Cell signaling). Membranes were blotted with primary antibody overnight at 4°C at a dilution of 1:1000. Proteins were visualized with enhanced chemiluminescence reagents (ECL/ECL Plus, Amersham GE) and Kodak X-OMAT film.

Immunohistochemistry in mouse liver specimens

Liver tissue from euthanized mice was fixed in 4% formalin for 48h, embedded in paraffin, and sectioned into 3–5 µm slices. Formalin fixed, paraffin-embedded mouse tumor and adjacent liver sections were deparaffinized, hydrated and incubated with primary antibody overnight at 4°C. Sections were stained with antibody for CK19 (Cell signaling, 12434, 1:500), Pan-CK (Cell signaling, C11, 1:500) or TUNEL (ApopTag® Peroxidase In Situ Apoptosis detection kit (EMD Millipore). Primary antibody was detected with HRP-conjugated secondary antibody and diaminobenzidine (Dako, Carpentaria, CA, USA). Liver tissue sections were counterstained with hematoxylin.

Statistical analysis

Experimental statistical analyses were performed using GraphPad Prism software. Student two-tailed *t* test, log-rank (Mantel–Cox) test, and one-way ANOVA (with Bonferroni *post hoc* test) were used throughout as indicated in the text. Data were considered statistically significant at $P < 0.05$.

Acknowledgments:
This publication was made possible through support by core facilities at the Mayo Clinic including Medical Genome Facility Gene Analysis Core, Pathology Research Core, and the Antibody Hybridoma Core.

Grant Support:
E. Loeuillard was supported by the Cholangiocarcinoma Foundation. S.I. Ilyas was supported by the NIH/NCI (1K08CA236874), American Gastroenterology Association Research Scholar Award, Mayo Center for Cell Signaling in Gastroenterology (Pilot & Feasibility Award P30DK084567), the Mayo Hepatobiliary Cancer SPORE (P50 CA210964) Career Enhancement Program, the Satter Family Liver Cancer Award, and the Mayo Foundation.

References

1 von Karstedt, S., Montinaro, A. & Walczak, H. Exploring the TRAILs less travelled: TRAIL in cancer biology and therapy. *Nat Rev Cancer* **17**, 352-366, doi:10.1038/nrc.2017.28 (2017).

2 Pan, G. *et al.* The receptor for the cytotoxic ligand TRAIL. *Science* **276**, 111-113, doi:10.1126/science.276.5309.111 (1997).

3 Walczak, H. *et al.* TRAIL-R2: a novel apoptosis-mediating receptor for TRAIL. *EMBO J* **16**, 5386-5397, doi:10.1093/emboj/16.17.5386 (1997).

4 Wu, G. S., Burns, T. F., Zhan, Y., Alnemri, E. S. & El-Deiry, W. S. Molecular cloning and functional analysis of the mouse homologue of the KILLER/DR5 tumor necrosis factor-related apoptosis-inducing ligand (TRAIL) death receptor. *Cancer Res* **59**, 2770-2775 (1999).

5 Smyth, M. J. *et al.* Tumor necrosis factor-related apoptosis-inducing ligand (TRAIL) contributes to interferon gamma-dependent natural killer cell protection from tumor metastasis. *J Exp Med* **193**, 661-670, doi:10.1084/jem.193.6.661 (2001).

6 Condamine, T. *et al.* ER stress regulates myeloid-derived suppressor cell fate through TRAIL-R-mediated apoptosis. *J Clin Invest* **124**, 2626-2639, doi:10.1172/JCI74056 (2014).

7 Nalawade, S. A. *et al.* Selectively targeting myeloid-derived suppressor cells through TRAIL receptor 2 to enhance the efficacy of CAR T cell therapy for treatment of breast cancer. *J Immunother Cancer* **9**, doi:10.1136/jitc-2021-003237 (2021).

8 Hartwig, T. *et al.* The TRAIL-Induced Cancer Secretome Promotes a Tumor-Supportive Immune Microenvironment via CCR2. *Mol Cell* **65**, 730-742 e735, doi:10.1016/j.molcel.2017.01.021 (2017).

9 Ishimura, N., Isomoto, H., Bronk, S. F. & Gores, G. J. Trail induces cell migration and invasion in apoptosis-resistant cholangiocarcinoma cells. *Am J Physiol Gastrointest Liver Physiol* **290**, G129-136, doi:10.1152/ajpgi.00242.2005 (2006).

10 Trauzold, A. *et al.* TRAIL promotes metastasis of human pancreatic ductal adenocarcinoma. *Oncogene* **25**, 7434-7439, doi:10.1038/sj.onc.1209719 (2006).

11 von Karstedt, S. *et al.* Cancer cell-autonomous TRAIL-R signaling promotes KRAS-driven cancer progression, invasion, and metastasis. *Cancer Cell* **27**, 561-573, doi:10.1016/j.ccell.2015.02.014 (2015).

12 Schneider, P. *et al.* TRAIL receptors 1 (DR4) and 2 (DR5) signal FADD-dependent apoptosis and activate NF-kappaB. *Immunity* **7**, 831-836, doi:10.1016/s1074-7613(00)80401-x (1997).

13 Azijli, K., Weyhenmeyer, B., Peters, G. J., de Jong, S. & Kruyt, F. A. Non-canonical kinase signaling by the death ligand TRAIL in cancer cells: discord in the death receptor family. *Cell Death Differ* **20**, 858-868, doi:10.1038/cdd.2013.28 (2013).

14 Rizvi, S., Khan, S. A., Hallemeier, C. L., Kelley, R. K. & Gores, G. J. Cholangiocarcinoma - evolving concepts and therapeutic strategies. *Nat Rev Clin Oncol* **15**, 95-111, doi:10.1038/nrclinonc.2017.157 (2018).

15 Piha-Paul, S. A. *et al.* Efficacy and safety of pembrolizumab for the treatment of advanced biliary cancer: Results from the KEYNOTE-158 and KEYNOTE-028 studies. *Int J Cancer* **147**, 2190-2198, doi:10.1002/ijc.33013 (2020).

16 Ho, W. J., Jaffee, E. M. & Zheng, L. The tumour microenvironment in pancreatic cancer - clinical challenges and opportunities. *Nat Rev Clin Oncol* **17**, 527-540, doi:10.1038/s41571-020-0363-5 (2020).
17 Loeuillard, E. *et al.* Targeting tumor-associated macrophages and granulocytic myeloid-derived suppressor cells augments PD-1 blockade in cholangiocarcinoma. *J Clin Invest* **130**, 5380-5396, doi:10.1172/JCI137110 (2020).
18 Veglia, F., Perego, M. & Gabrilovich, D. Myeloid-derived suppressor cells coming of age. *Nat Immunol* **19**, 108-119, doi:10.1038/s41590-017-0022-x (2018).
19 Hawila, E. *et al.* CCR5 Directs the Mobilization of CD11b(+)Gr1(+)Ly6C(low) Polymorphonuclear Myeloid Cells from the Bone Marrow to the Blood to Support Tumor Development. *Cell Rep* **21**, 2212-2222, doi:10.1016/j.celrep.2017.10.104 (2017).
20 Filipazzi, P. *et al.* Identification of a new subset of myeloid suppressor cells in peripheral blood of melanoma patients with modulation by a granulocyte-macrophage colony-stimulation factor-based antitumor vaccine. *J Clin Oncol* **25**, 2546-2553, doi:10.1200/JCO.2006.08.5829 (2007).
21 Kaneda, M. M. *et al.* PI3Kgamma is a molecular switch that controls immune suppression. *Nature* **539**, 437-442, doi:10.1038/nature19834 (2016).
22 Meyer, C. *et al.* Frequencies of circulating MDSC correlate with clinical outcome of melanoma patients treated with ipilimumab. *Cancer Immunol Immunother* **63**, 247-257, doi:10.1007/s00262-013-1508-5 (2014).
23 Salvagno, C. *et al.* Therapeutic targeting of macrophages enhances chemotherapy efficacy by unleashing type I interferon response. *Nat Cell Biol* **21**, 511-521, doi:10.1038/s41556-019-0298-1 (2019).
24 Evans, R. *et al.* Integrins in immunity. *J Cell Sci* **122**, 215-225, doi:10.1242/jcs.019117 (2009).
25 Liu, X. *et al.* Endogenous tumor-reactive CD8(+) T cells are differentiated effector cells expressing high levels of CD11a and PD-1 but are unable to control tumor growth. *Oncoimmunology* **2**, e23972, doi:10.4161/onci.23972 (2013).
26 Cardoso Alves, L., Corazza, N., Micheau, O. & Krebs, P. The multifaceted role of TRAIL signaling in cancer and immunity. *FEBS J*, doi:10.1111/febs.15637 (2020).
27 Maekawa, Y. *et al.* Notch2 integrates signaling by the transcription factors RBP-J and CREB1 to promote T cell cytotoxicity. *Nat Immunol* **9**, 1140-1147, doi:10.1038/ni.1649 (2008).
28 Clausen, B. E., Burkhardt, C., Reith, W., Renkawitz, R. & Forster, I. Conditional gene targeting in macrophages and granulocytes using LysMcre mice. *Transgenic Res* **8**, 265-277, doi:10.1023/a:1008942828960 (1999).
29 Marigo, I. *et al.* Tumor-induced tolerance and immune suppression depend on the C/EBPbeta transcription factor. *Immunity* **32**, 790-802, doi:10.1016/j.immuni.2010.05.010 (2010).
30 Luo, J. L., Kamata, H. & Karin, M. IKK/NF-kappaB signaling: balancing life and death--a new approach to cancer therapy. *J Clin Invest* **115**, 2625-2632, doi:10.1172/JCI26322 (2005).
31 Dondelinger, Y. *et al.* NF-kappaB-Independent Role of IKKalpha/IKKbeta in Preventing RIPK1 Kinase-Dependent Apoptotic and Necroptotic Cell Death during TNF Signaling. *Mol Cell* **60**, 63-76, doi:10.1016/j.molcel.2015.07.032 (2015).

32 Ni, J. *et al.* Single-Cell RNA Sequencing of Tumor-Infiltrating NK Cells Reveals that Inhibition of Transcription Factor HIF-1alpha Unleashes NK Cell Activity. *Immunity* **52**, 1075-1087 e1078, doi:10.1016/j.immuni.2020.05.001 (2020).
33 Murakami, S. *et al.* Yes-associated protein mediates immune reprogramming in pancreatic ductal adenocarcinoma. *Oncogene* **36**, 1232-1244, doi:10.1038/onc.2016.288 (2017).
34 Ehrhardt, H. *et al.* TRAIL induced survival and proliferation in cancer cells resistant towards TRAIL-induced apoptosis mediated by NF-kappaB. *Oncogene* **22**, 3842-3852, doi:10.1038/sj.onc.1206520 (2003).
35 Fulda, S. The dark side of TRAIL signaling. *Cell Death Differ* **20**, 845-846, doi:10.1038/cdd.2013.36 (2013).
36 Boi, S. K. *et al.* Obesity diminishes response to PD-1-based immunotherapies in renal cancer. *J Immunother Cancer* **8**, doi:10.1136/jitc-2020-000725 (2020).
37 Norian, L. A. *et al.* Eradication of metastatic renal cell carcinoma after adenovirus-encoded TNF-related apoptosis-inducing ligand (TRAIL)/CpG immunotherapy. *PLoS One* **7**, e31085, doi:10.1371/journal.pone.0031085 (2012).
38 Hendriks, D. *et al.* Programmed Death Ligand 1 (PD-L1)-targeted TRAIL combines PD-L1-mediated checkpoint inhibition with TRAIL-mediated apoptosis induction. *Oncoimmunology* **5**, e1202390, doi:10.1080/2162402X.2016.1202390 (2016).
39 James, B. R., Brincks, E. L., Kucaba, T. A., Boon, L. & Griffith, T. S. Effective TRAIL-based immunotherapy requires both plasmacytoid and CD8alpha dendritic cells. *Cancer Immunol Immunother* **63**, 685-697, doi:10.1007/s00262-014-1548-5 (2014).
40 Yamada, D. *et al.* IL-33 facilitates oncogene-induced cholangiocarcinoma in mice by an interleukin-6-sensitive mechanism. *Hepatology* **61**, 1627-1642, doi:10.1002/hep.27687 (2015).
41 Rizvi, S. *et al.* YAP-associated chromosomal instability and cholangiocarcinoma in mice. *Oncotarget* **9**, 5892-5905, doi:10.18632/oncotarget.23638 (2018).
42 O'Dell, M. R. *et al.* Kras(G12D) and p53 mutation cause primary intrahepatic cholangiocarcinoma. *Cancer Res* **72**, 1557-1567, doi:10.1158/0008-5472.CAN-11-3596 (2012).
43 Tannapfel, A. *et al.* Frequency of p16(INK4A) alterations and K-ras mutations in intrahepatic cholangiocarcinoma of the liver. *Gut* **47**, 721-727, doi:10.1136/gut.47.5.721 (2000).
44 Tannapfel, A. *et al.* Mutations of p53 tumor suppressor gene, apoptosis, and proliferation in intrahepatic cholangiocellular carcinoma of the liver. *Dig Dis Sci* **45**, 317-324, doi:10.1023/a:1005412626515 (2000).
45 Younger, N. T. *et al.* In Vivo Modeling of Patient Genetic Heterogeneity Identifies New Ways to Target Cholangiocarcinoma. *Cancer Res* **82**, 1548-1559, doi:10.1158/0008-5472.CAN-21-2556 (2022).
46 Wang, J. *et al.* Loss of Fbxw7 synergizes with activated Akt signaling to promote c-Myc dependent cholangiocarcinogenesis. *J Hepatol* **71**, 742-752, doi:10.1016/j.jhep.2019.05.027 (2019).

FIGURE LEGENDS

Figure 1 TRAIL-R$^+$ immune cells in the TIME are essential in facilitating tumor progression. (**A**-**B**) UMAP plots show cells defined as positive cells (red dots) for UMI of the specific gene larger than 1.7. *TNFSF10* positive human CCA tumor cells in human CCA (GSE210066, GSE189903, GSE138709, GSE125449, HRA000863). *TNFRSF10A* positive cells (left panel) and *TNFRSF10B* positive cell (right panel) in immune cells. (**C**) Schematic of *Trail-r^{-l-}* mouse model of CCA implanted with SB cells. (**D**) Average tumor weight in mg of WT *or Trail-r^{-l-}* mice ($n \geq 44$). (**E**) Representative photographs of livers from **D**. (**F**) Schematic of *Trail-r^{-l-}* mouse model of CCA implanted with KPPC cells. (**G**) Average tumor weight in mg of WT *or Trail-r^{-l-}* mice (n =12). (**H**) Representative photographs of livers from **G**. (**I**) Schematic of *Trail-r^{-l-}* mouse model of CCA implanted with FAC cells. (**J**) Average tumor weight in mg of WT *or Trail-r^{-l-}* mice (n = 4). (**K**) Representative photographs of livers from **J**. Data are represented as mean ± SD. Unpaired Student's *t* test was used. *$P < 0.05$.

Figure 2 Genetic deletion of *Trail-r* augments CTL infiltration and function. (**A**–**G**) Tumor harvested 28 days after orthotopic implantation of 7.5×10^5 SB cells or 14 days after orthotopic implantation of 7.5×10^5 KPPC cells in WT or *Trail-r$^{-/-}$* mouse livers. (**A**) Percentage of CTLs in CD45$^+$ cell population (CD45$^+$ CD3$^+$ CD8$^+$) in adjacent liver and SB cell tumors from WT and *Trail-r$^{-/-}$* mice ($n \geq 5$). (**B**) Percentage of CTLs in CD45$^+$ cell population (CD45$^+$ CD3$^+$ CD8$^+$) in adjacent liver and KPPC cell tumors from WT and *Trail-r$^{-/-}$* mice ($n \geq 3$). (**C**) Percentage of reactive CTLs in CD45$^+$ cell population (CD45$^+$ CD3$^+$ CD8$^+$ CD11a$^+$) in adjacent liver and SB cell tumors from WT and *Trail-r$^{-/-}$* mice ($n \geq 5$). (**D**) Percentage of reactive CTLs in CD45$^+$ cell population (CD45$^+$ CD3$^+$ CD8$^+$ CD11a$^+$) in adjacent liver and KPPC cell tumors from WT and *Trail-r$^{-/-}$* mice ($n \geq 3$). (**E**) Percentage of reactive CTL Granzyme B$^+$ in adjacent liver and SB cell tumors from WT and *Trail-r$^{-/-}$* mice ($n \geq 9$). (**F**) Percentage of apoptotic reactive CTL (7AAD$^+$ Annexin V$^+$) in adjacent liver and SB cell tumors from WT and *Trail-r$^{-/-}$* mice ($n \geq 5$). (**G**) Percentage of proliferative reactive CTL (Ki67$^+$) in adjacent liver and SB cell tumors from WT and *Trail-r$^{-/-}$* mice ($n \geq 5$). (**H**) Schematic of in vitro CD8$^+$ T cell coculture experiment. (**I**) Percentage of CD8$^+$ T cell proliferation (Ki67$^+$ cells from CD3$^+$ CD8$^+$ cells) (right panel), of CD8$^+$ T cell apoptosis (7AAD$^+$ AnnexinV$^+$ cells from CD3$^+$ CD8$^+$ cells) (middle panel) and ratio of proliferation/apoptosis (left panel) after 36h of coculture with SB cells ($n \geq 5$). (**J**) Schematic of ΔCD8 mouse model of CCA implanted with SB cells. (**K**) Average tumor weight in mg of *f/f or* ΔCD8 mice ($n \geq 3$). (**L**) Representative photographs of livers from **K**. Data are represented as mean ± SD. Unpaired Student's *t* test was used. ns=nonsignificant; *$P < 0.05$; **$P < 0.01$; ***$P < 0.001$.

Figure 3 TRAIL-TRAIL-R augments MDSCs abundance via enhanced proliferation. (**A**) Percentage of G-MDSCs (CD45$^+$ F4/80$^-$ CD11b$^+$ CD11c$^-$ Ly6C$^-$ Ly6G$^+$) (left panel) and M-MDSCs (CD45$^+$ F4/80$^-$ CD11b$^+$ CD11c$^-$ Ly6C$^+$ Ly6G$^-$) (right panel) in normal liver, adjacent liver and SB tumors from WT and *Trail-r$^{-/-}$* mice ($n \geq 5$). (**B**) Percentage of G-MDSCs (left panel) and M-MDSCs (right panel) in adjacent liver and KPPC tumors from WT and *Trail-r$^{-/-}$* mice ($n \geq 4$). (**C**) Schematic of *LyzM^{cre}Trail-r$^{f/f}$* mouse model of CCA. (**D**) Average tumor weight in mg of *LyzM^{cre}* (f/f) or *LyzM^{cre}Trail-r$^{f/f}$* (Δmye) mice ($n \geq 8$). (**E**) Representative photographs of livers from **D.** (**F**) Percentage of CTLs and reactive CTLs in CD45$^+$ cell population in SB tumors from f/f and Δmye mice ($n \geq 8$). (**G**) percentage of G-MDSCs in CD45$^+$ cell population SB tumors from f/f and Δmye mice ($n \geq 6$). (**H**) percentage of M-MDSCs in CD45$^+$ cell population SB tumors from f/f and Δmye mice ($n \geq 6$). Data are represented as mean ± SD. Unpaired Student's *t* test was used. ns=nonsignificant; *$P < 0.05$; ***$P < 0.001$.

Figure 4 TRAIL-TRAIL-R augments MDSCs abundance via enhanced proliferation. (**A**) Percentage of apoptosis and (**B**) proliferation in G-MDSCs in adjacent liver and SB tumors from WT and *Trail-r$^{-/-}$* mice ($n \geq 4$). (**C**) Percentage of apoptosis and (**D**) proliferation in G-MDSCs in SB tumors from f/f and Δmye mice ($n \geq 11$). (**E**) Schematic of in vitro MDSC cell coculture experiment and western blot of TRAIL-R in MDSCs isolated from WT and *Trail-r$^{-/-}$* mice (**F**) Percentage of MDSC cell proliferation

(Ki67$^+$ cells from CD11b$^+$ Gr-1$^+$ cells) after 48h of coculture with SB cells ($n \geq 9$). Data are represented as mean ± SD. Unpaired Student's *t* test was used. ns=nonsignificant; *$P < 0.05$; **$P < 0.01$; ***$P < 0.001$.

Figure 5 Non-canonical TRAIL-R signaling promotes MDSC survival in an NF-κB dependant manner. (**A**) Kinetics of NF-kB activation pathway by western blot of P65 subunit in nuclear fraction of WT and *Trail-r*$^{-/-}$ MDSCs after SB1 medium stimulation. (**B**) Schematic of in vitro induced MDSC cell from WT mice treated with TPCA-1, an inhibitor of NF-κB pathway, coculture with SB cells experiment. (**C**) Percentage of MDSC cell apoptosis (left panel) (7AAD$^+$ annexin V$^+$ cells from CD11b$^+$ Gr-1$^+$ cells) and proliferation (right panel) (Ki67$^+$ cells from CD11b$^+$ Gr-1$^+$ cells) after 48h of coculture ($n \geq 6$). Data are represented as mean ± SD. Unpaired Student's *t* test was used. ***$P < 0.001$. (**D**) Seurat module score for NF-kB pathway[32] was examined in tumors from three murine CCA models using single cell RNA sequencing data. NF-kB pathway variations across different cell types, as determined by a one-way ANOVA test (adjusted $p < 0.05$, using Tukey's multiple comparisons test).

Figure 6 TRAIL-TRAIL-R has pleiotropic effects on the CCA TIME. (**A**) Schematic of WT mouse model of CCA implanted with SB cells generated by CRISPR-Cas9-mediated knockdown of a non-target (NT), *Trail* (SB-*Trail*$^{-/-}$) or TRAIL-R (SB-*Trail-r*$^{-/-}$). (**B**) Average tumor weight in mg of WT mice implanted with SB-NT, SB-*Trail*$^{-/-}$ or SB-*Trail-r*$^{-/-}$ ($n \geq 17$). (**C**) Representative photographs of livers from **B**. (**D**) Percentage of G-MDSCs (CD45$^+$ F4/80$^-$ CD11b$^+$ CD11c$^-$ Ly6C$^-$ Ly6G$^+$) in adjacent liver and tumors from WT implanted with SB-NT or SB-*Trail*$^{-/-}$ ($n \geq 4$). (**E**) Percentage of M-MDSCs (CD45$^+$ F4/80$^-$ CD11b$^+$ CD11c$^-$ Ly6G$^-$ Ly6C$^+$) in adjacent liver and tumors from WT implanted with SB-NT or SB-*Trail*$^{-/-}$ ($n \geq 4$). (**F**) Percentage of CTLs in CD45$^+$ cell population (CD45$^+$ CD3$^+$ CD8$^+$) in adjacent liver and tumors from WT mice implanted with SB-NT or SB-*Trail*$^{-/-}$ ($n \geq 4$). (**G**) Percentage of reactive CTLs in CD45$^+$ cell population (CD45$^+$ CD3$^+$ CD8$^+$ CD11a$^+$) in adjacent liver and tumors from WT mice implanted with SB-NT or SB-*Trail*$^{-/-}$ ($n \geq 4$). (**H**) Schematic of in vitro MDSC cell coculture with SB-NT or SB-*Trail*$^{-/-}$ experiment. (**I**) Percentage of MDSC cell apoptosis (left panel) (7AAD$^+$ annexin V$^+$ cells from CD11b$^+$ Gr-1$^+$ cells) and proliferation (right panel) (Ki67$^+$ cells from CD11b$^+$ Gr-1$^+$ cells) after 48h of coculture ($n \geq 9$). (**J**) Expression of two probes targeting TNFSF10 in 20 patients with high expression of MDSC marker (MDSC_high) and 20 patients with low expression of MDSC marker (MDSC_low). Data are represented as mean ± SD. Unpaired Student's *t* test was used. ns=nonsignificant; *$P < 0.05$; **$P < 0.01$.

Supplementary Figure S1. (**A**) Immunoblot analysis of TRAIL expression in SB, KRAS and FAC mouse CCA cell lysates (**B**) Representative photomicrographs of hematoxylin and eosin-stained (left panel) and CK19 IHC (right panel) of SB tumor section from WT and *Trail-r*$^{-/-}$ mice. Scale bar, 50um. (**C**) Representative photomicrographs of hematoxylin and eosin-stained (left panel) and Pan-keratin IHC (right panel) of KPPC tumor section from WT and *Trail-r*$^{-/-}$ mice. Scale bar, 50um.

Supplementary Figure S2. (**A**–**C**) Tumor harvested 28 days after orthotopic implantation of 7.5×10^5 SB cells in WT or *Trail-r*$^{-/-}$ mouse livers. (**A**) Percentage of reactive CD8$^+$ PD-1$^+$ in normal liver, adjacent liver and SB cell tumors from WT and *Trail-r*$^{-/-}$ mice ($n \geq 5$). (**B**) Percentage of CD4$^+$ T cells in CD45$^+$ cell population (CD45$^+$ CD3$^+$ CD4$^+$) in normal liver, adjacent liver and SB cell tumors from WT and *Trail-r*$^{-/-}$ mice ($n \geq 5$). (**C**) Percentage of natural killer (NK) cells in CD45$^+$ cell population (CD45$^+$ CD3$^-$ NK1.1$^+$) in normal liver, adjacent liver and SB cell tumors from WT and *Trail-r*$^{-/-}$ mice ($n \geq 5$). (**D**) Percentage of activation markers CD69$^+$; (**E**) INFγ$^+$; (**F**) TIM3$^+$ and (**G**) PD-1$^+$ in CD8$^+$ T cell population after 36h of coculture with SB cells ($n \geq 5$). Data are represented as mean ± SD. Unpaired Student's *t* test was used. ns=nonsignificant; **$P < 0.01$.

Supplementary Figure S3 (**A**–**C**) Tumor harvested 28 days after orthotopic implantation of 7.5×10^5 SB cells in WT or *Trail-r*$^{-/-}$ mouse livers. (**A**) Percentage of macrophages (CD45$^+$ F4/80$^+$ CD11b$^+$) in CD45$^+$

cell population in normal liver, adjacent liver and SB tumors from WT and *Trail-r*$^{-/-}$ mice ($n \geq 5$). (**B**) Percentage of TAMs (CD45$^+$ F4/80$^+$ CD11b$^+$ CD206$^+$) (left panel) and M1-like macrophages (CD45$^+$ F4/80$^+$ CD11b$^+$ CD11c$^+$) (right panel) in CD45$^+$ cell population in normal liver, adjacent liver and SB tumors from WT and *Trail-r*$^{-/-}$ mice ($n \geq 5$). (**C**) Percentage of dendritic cells (CD45$^+$ F4/80$^-$ CD11b$^+$ CD11c$^+$) in CD45$^+$ cell population in normal liver, adjacent liver and SB tumors from WT and *Trail-r*$^{-/-}$ mice ($n \geq 5$). (**D**–**E**) Tumor harvested 14 days after orthotopic implantation of 7.5×10^5 KPPC cells in WT or *Trail-r*$^{-/-}$ mouse livers. (**D**) Percentage of macrophages (CD45$^+$ F4/80$^+$ CD11b$^+$) in CD45$^+$ cell population in adjacent liver and KPPC tumors from WT and *Trail-r*$^{-/-}$ mice ($n \geq 4$). (**E**) Percentage of TAMs (CD45$^+$ F4/80$^+$ CD11b$^+$ CD206$^+$) (left panel) and M1-like macrophages (CD45$^+$ F4/80$^+$ CD11b$^+$ CD11c$^+$) (right panel) in CD45$^+$ cell population in adjacent liver and KPPC tumors from WT and *Trail-r*$^{-/-}$ mice ($n \geq 4$). (**F**–**G**) Tumor harvested 28 days after orthotopic implantation of 7.5×10^5 SB cells in f/f and Δmye mouse livers (**F**) Percentage of macrophages (CD45$^+$ F4/80$^+$ CD11b$^+$) in CD45$^+$ cell population in adjacent liver and SB tumors from f/f and Δmye mice ($n \geq 6$). (**G**) Percentage of M1-like macrophages (CD45$^+$ F4/80$^+$ CD11b$^+$ CD11c$^+$) in CD45$^+$ cell population in adjacent liver and SB tumors from f/f and Δmye mice ($n \geq 6$). Data are represented as mean ± SD. Unpaired Student's *t* test was used. ns=nonsignificant; $^{**}P < 0.01$; $^{***}P < 0.001$.

Supplementary Figure S4 (**A**) Percentage of apoptosis and (**B**) proliferation in M-MDSCs in adjacent liver and SB tumors from WT and *Trail-r*$^{-/-}$ mice ($n \geq 4$). (**C**) Percentage of G-MDSCs Arginase 1$^+$ (left panel) and IL-10$^+$ (right panel) in adjacent liver and SB tumors from WT and *Trail-r*$^{-/-}$ mice ($n \geq 4$). (**D**) Percentage of M-MDSCs Arginase 1$^+$ (left panel) and IL-10$^+$ (right panel) in adjacent liver and SB tumors from WT and *Trail-r*$^{-/-}$ mice ($n \geq 4$). (**E**) Percentage of G-MDSCs Arginase 1$^+$ (left panel) and IL-10$^+$ (right panel) in adjacent liver and SB tumors from f/f and Δmye mice ($n \geq 6$). (**F**) Percentage of M-MDSCs Arginase 1$^+$ (left panel) and IL-10$^+$ (right panel) in adjacent liver and SB tumors from f/f and Δmye mice ($n \geq 6$). Data are represented as mean ± SD. Unpaired Student's *t* test was used. ns=nonsignificant

Supplementary Figure S5 (**A**) Representative pictures of confocal immunofluorescence image of MDSCs cocultured with SB cells for 24h and treated with TPCA-1; pan-keratin (green), CD45 (red), NF-kB (white) and DAPI. Scale bar = 20um. (**B**) Unsupervised clustering of single cell RNA sequencing of murine immune cells in 3 different CCA models revealed 35 cell clusters. UMAP plot demonstrates immune cell clusters.

Supplementary Figure S6 (**A**) Representative photomicrographs of hematoxylin and eosin-stained (left panel) and CK19 IHC (right panel) of SB tumor section from WT mice implanted with SB-NT, SB-*Trail*$^{-/-}$ or SB-*Trail-r*$^{-/-}$. (**B**) Percentage of macrophages in CD45$^+$ cell population (CD45$^+$ F4/80$^+$ CD11b$^+$) in adjacent liver and tumors from WT implanted with SB-NT or SB-*Trail*$^{-/-}$ ($n \geq 4$). (**C**) Percentage of TAMs in CD45$^+$ cell population (CD45$^+$ F4/80$^+$ CD11b$^+$ CD206$^+$) in adjacent liver and tumors from WT implanted with SB-NT or SB-*Trail*$^{-/-}$ ($n \geq 4$). (**D**) Percentage of M1-like in CD45$^+$ cell population (CD45$^+$ F4/80$^+$ CD11b$^+$ CD11c$^+$) in adjacent liver and tumors from WT implanted with SB-NT or SB-*Trail*$^{-/-}$ ($n \geq 4$). (**E**) The normalized gene expression data for 92 CCA tumor samples from GSE76297. The expression of MDSC gene signature[33] was evaluated in the heatmap. Based on the heatmap, the 20 patients with highest expression of the MDSC signature are defined as MDSC high group and the 20 patients with lowest expression of the MDSC gene signature are defined as MDSC low group. Data are represented as mean ± SD. Unpaired Student's *t* test was used. ns=nonsignificant.

Figure 1

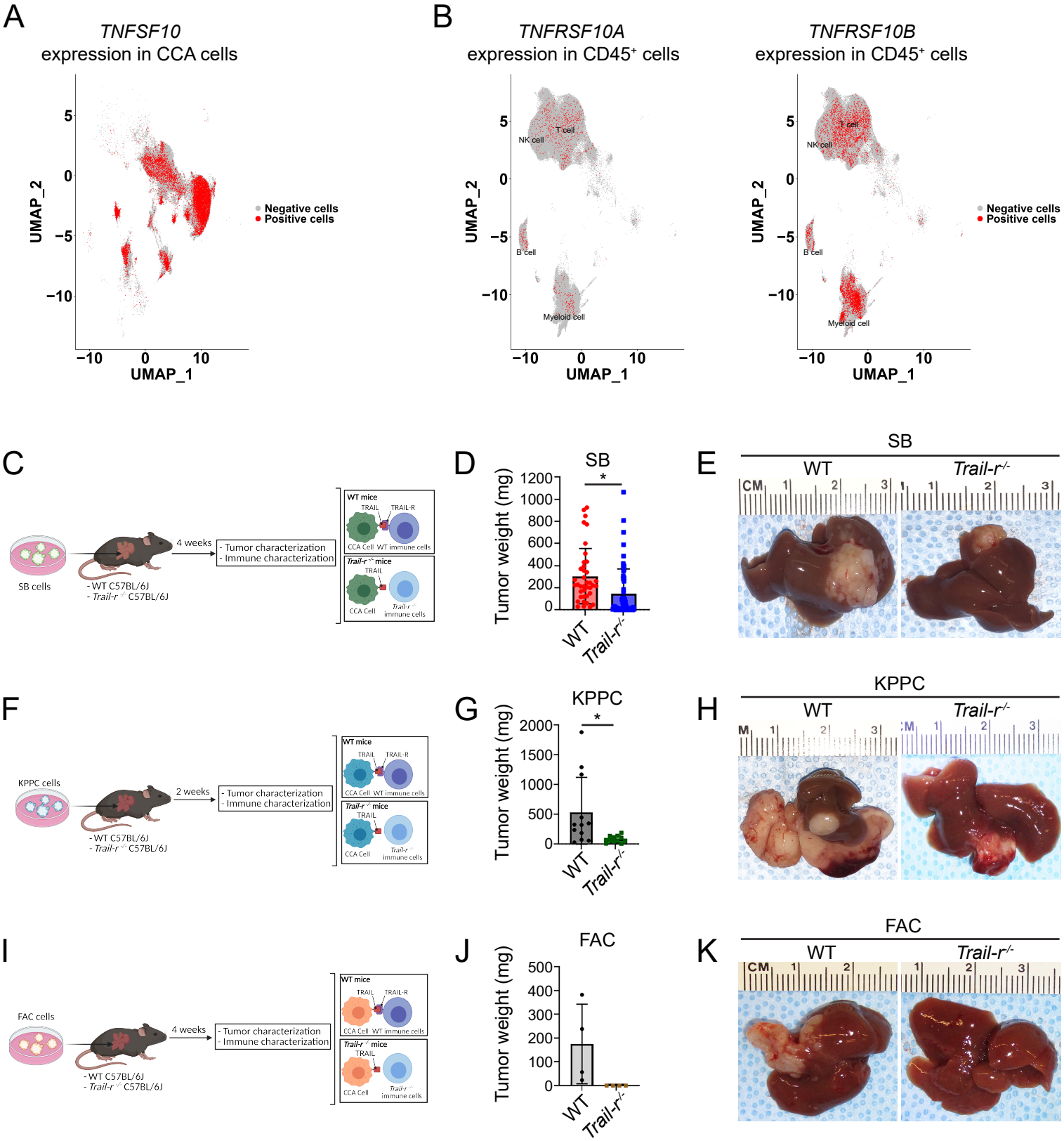
A
TNFSF10
expression in CCA cells
UMAP_2
UMAP_1
Negative cells
Positive cells
B
TNFRSF10A
expression in CD45+ cells
TNFRSF10B
expression in CD45+ cells
T cell
NK cell
B cell
Myeloid cell
C
SB cells
- WT C57BL/6J
- Trail-r-/- C57BL/6J
4 weeks
- Tumor characterization
- Immune characterization
WT mice
TRAIL
TRAIL-R
CCA Cell
WT immune cells
Trail-r-/- mice
Trail-r-/- immune cells
D
SB
Tumor weight (mg)
WT
Trail-r-/-
E
SB
WT
Trail-r-/-
F
KPPC cells
2 weeks
G
KPPC
H
I
FAC cells
J
FAC
K

Figure 2

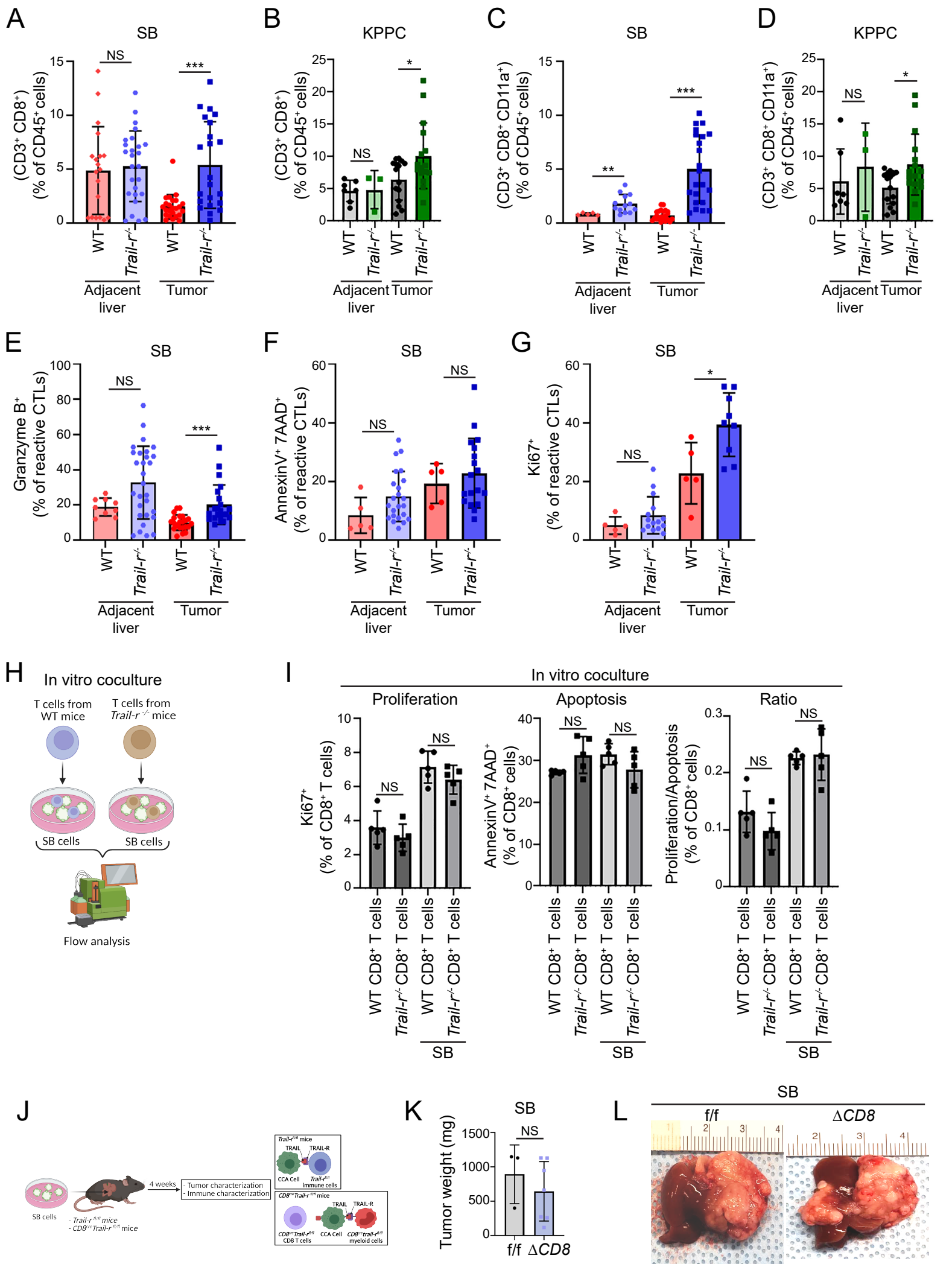
A
SB
(CD3+ CD8+) (% of CD45+ cells)
NS
***
WT
Trail-r-/-
Adjacent liver
Tumor
B
KPPC
*
C
SB
(CD3+ CD8+ CD11a+) (% of CD45+ cells)
**
D
KPPC
E
SB
Granzyme B+ (% of reactive CTLs)
F
SB
AnnexinV+ 7AAD+ (% of reactive CTLs)
G
SB
Ki67+ (% of reactive CTLs)
H
In vitro coculture
T cells from WT mice
T cells from Trail-r -/- mice
SB cells
Flow analysis
I
In vitro coculture
Proliferation
Apoptosis
Ratio
Ki67+ (% of CD8+ T cells)
AnnexinV+ 7AAD+ (% of CD8+ cells)
Proliferation/Apoptosis (% of CD8+ cells)
WT CD8+ T cells
Trail-r-/- CD8+ T cells
SB
J
SB cells
4 weeks
- Tumor characterization
- Immune characterization
TRAIL
TRAIL-R
CCA Cell
immune cells
CD8 T cells
myeloid cells
K
SB
Tumor weight (mg)
f/f
ΔCD8
L
SB
f/f
ΔCD8

Figure 3

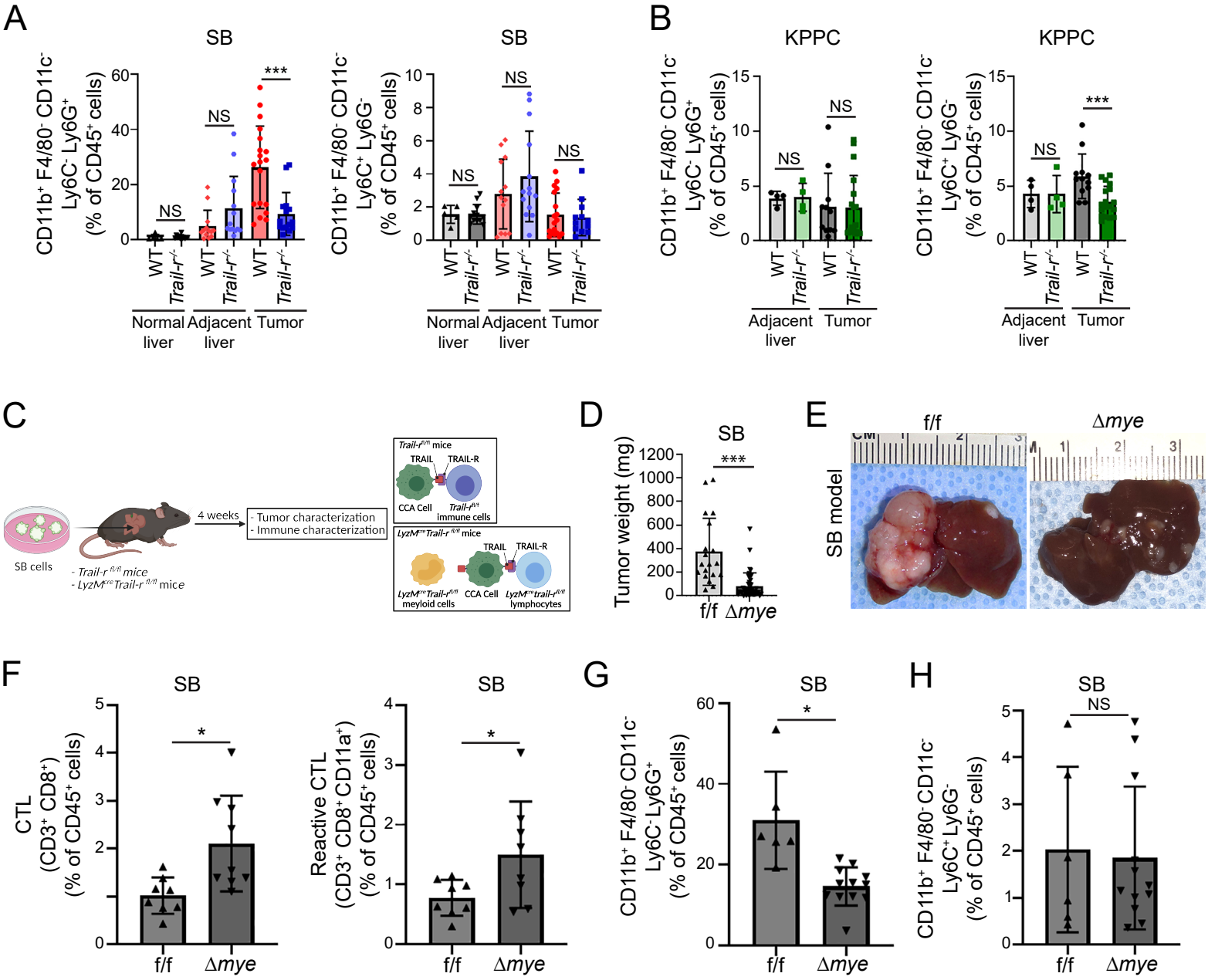
A
SB
CD11b+ F4/80- CD11c- Ly6C- Ly6G+ (% of CD45+ cells)
NS
***
WT
Trail-r-/-
Normal liver
Adjacent liver
Tumor
SB
CD11b+ F4/80- CD11c- Ly6C+ Ly6G- (% of CD45+ cells)
NS
B
KPPC
CD11b+ F4/80- CD11c- Ly6C- Ly6G+ (% of CD45+ cells)
Adjacent liver
Tumor
KPPC
CD11b+ F4/80- CD11c- Ly6C+ Ly6G- (% of CD45+ cells)
C
SB cells
- Trail-r fl/fl mice
- LyzMcre Trail-r fl/fl mice
4 weeks
- Tumor characterization
- Immune characterization
Trail-rfl/fl mice
TRAIL
TRAIL-R
CCA Cell
Trail-rfl/fl immune cells
LyzMcre Trail-rfl/fl mice
LyzMcre Trail-rfl/fl meyloid cells
CCA Cell
LyzMcre trail-rfl/fl lymphocytes
D
SB
Tumor weight (mg)
***
f/f
Δmye
E
f/f
Δmye
SB model
F
SB
CTL (CD3+ CD8+) (% of CD45+ cells)
*
f/f
Δmye
SB
Reactive CTL (CD3+ CD8+ CD11a+) (% of CD45+ cells)
*
G
SB
CD11b+ F4/80- CD11c- Ly6C- Ly6G+ (% of CD45+ cells)
*
H
SB
CD11b+ F4/80- CD11c- Ly6C+ Ly6G- (% of CD45+ cells)
NS

Figure 4

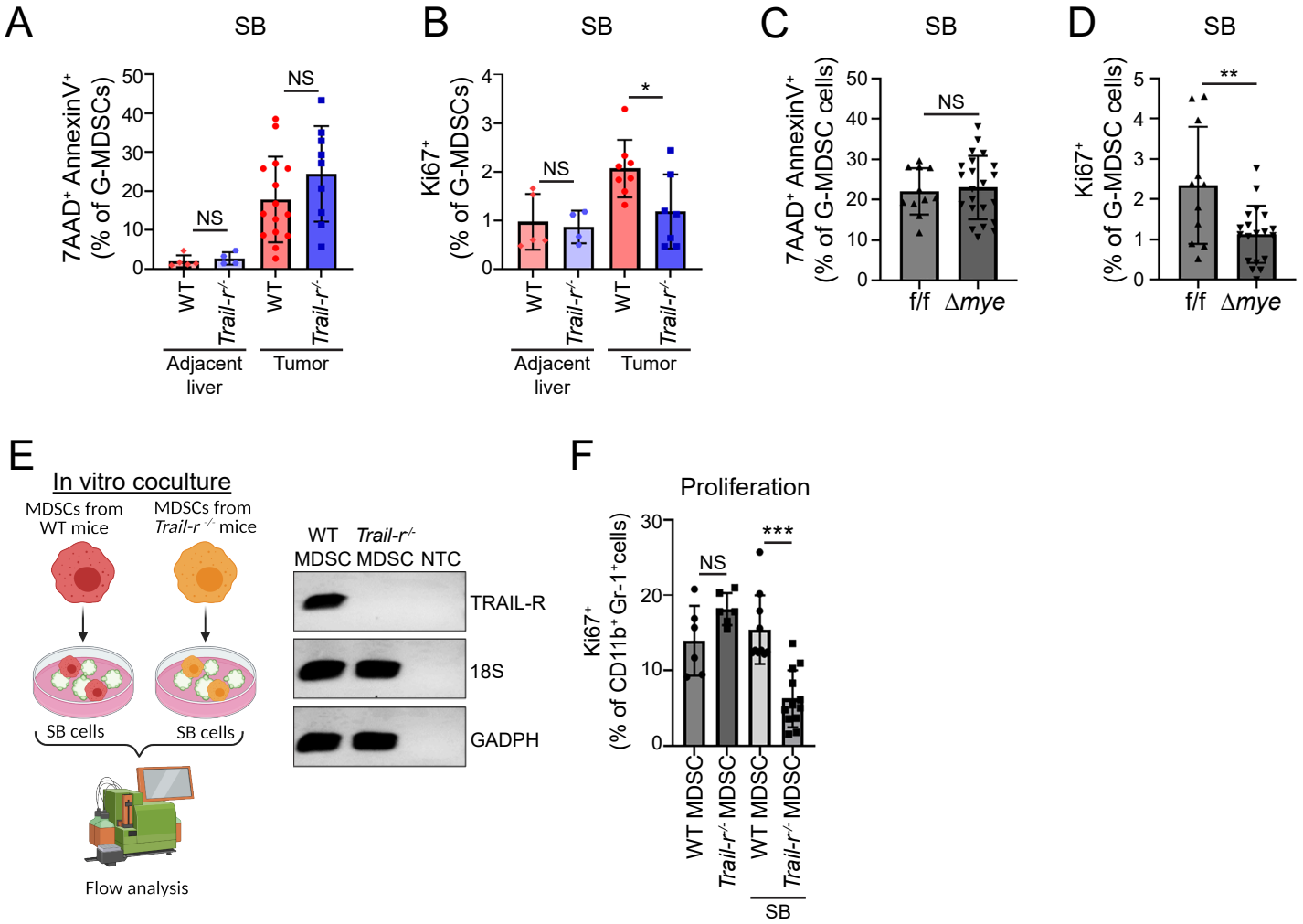
A
SB
7AAD+ AnnexinV+ (% of G-MDSCs)
NS
NS
WT
Trail-r-/-
WT
Trail-r-/-
Adjacent liver
Tumor
B
SB
Ki67+ (% of G-MDSCs)
NS
*
WT
Trail-r-/-
WT
Trail-r-/-
Adjacent liver
Tumor
C
SB
7AAD+ AnnexinV+ (% of G-MDSC cells)
NS
f/f
Δmye
D
SB
Ki67+ (% of G-MDSC cells)
**
f/f
Δmye
E
In vitro coculture
MDSCs from WT mice
MDSCs from Trail-r -/- mice
SB cells
SB cells
Flow analysis
WT MDSC
Trail-r-/- MDSC
NTC
TRAIL-R
18S
GADPH
F
Proliferation
Ki67+ (% of CD11b+ Gr-1+cells)
NS
***
WT MDSC
Trail-r-/- MDSC
WT MDSC
Trail-r-/- MDSC
SB

Figure 5

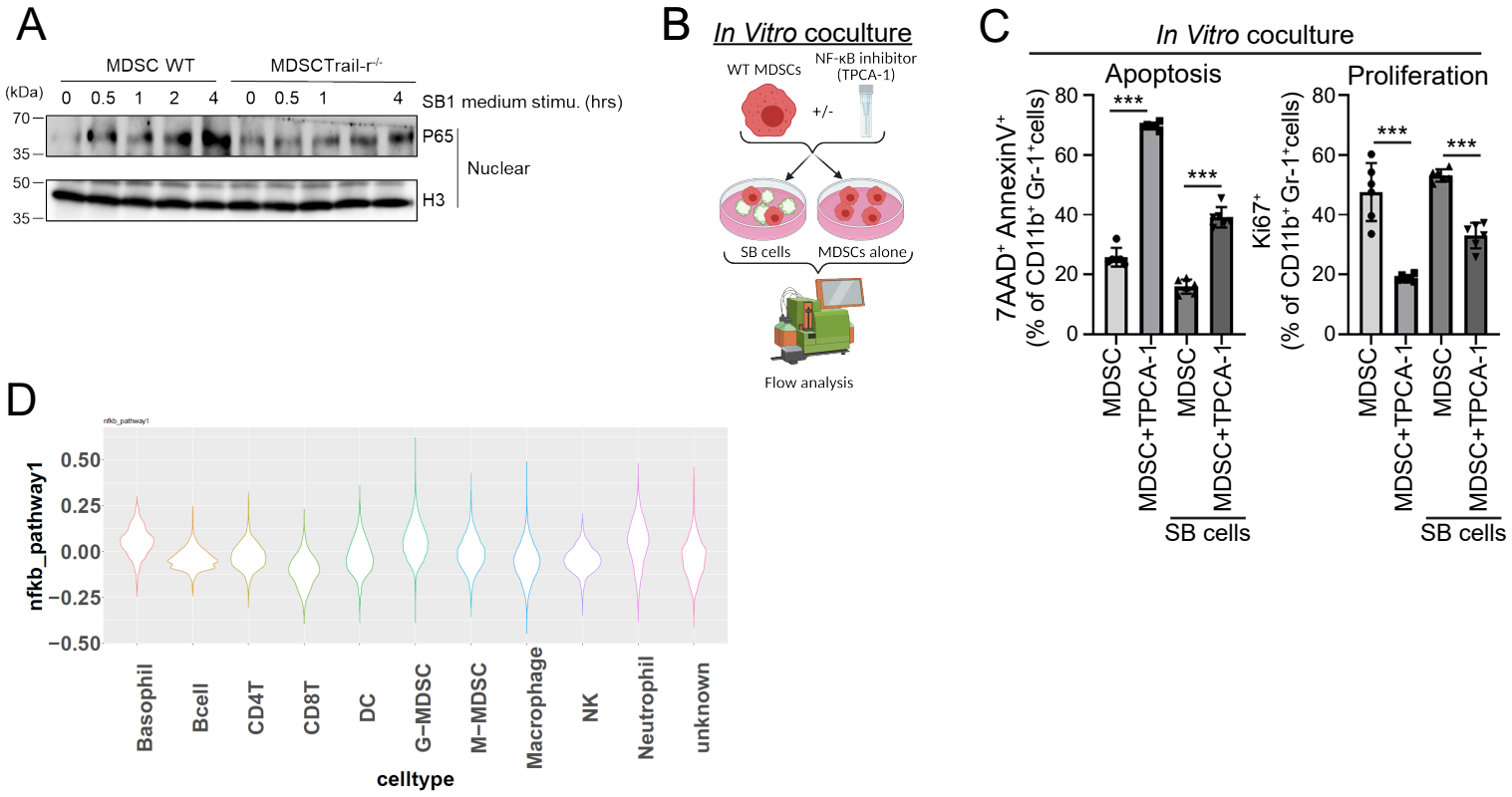
A
MDSC WT
MDSCTrail-r-/-
(kDa)
0 0.5 1 2 4 0 0.5 1 4
SB1 medium stimu. (hrs)
70
35
50
35
P65
H3
Nuclear
B
In Vitro coculture
WT MDSCs
NF-κB inhibitor (TPCA-1)
+/-
SB cells
MDSCs alone
Flow analysis
C
In Vitro coculture
Apoptosis
Proliferation
7AAD+ AnnexinV+ (% of CD11b+ Gr-1+cells)
Ki67+ (% of CD11b+ Gr-1+cells)
0
20
40
60
80
***
MDSC
MDSC+TPCA-1
MDSC
MDSC+TPCA-1
SB cells
D
nfkb_pathway1
0.50
0.25
0.00
−0.25
−0.50
Basophil
Bcell
CD4T
CD8T
DC
G−MDSC
M−MDSC
Macrophage
NK
Neutrophil
unknown
celltype

Figure 6

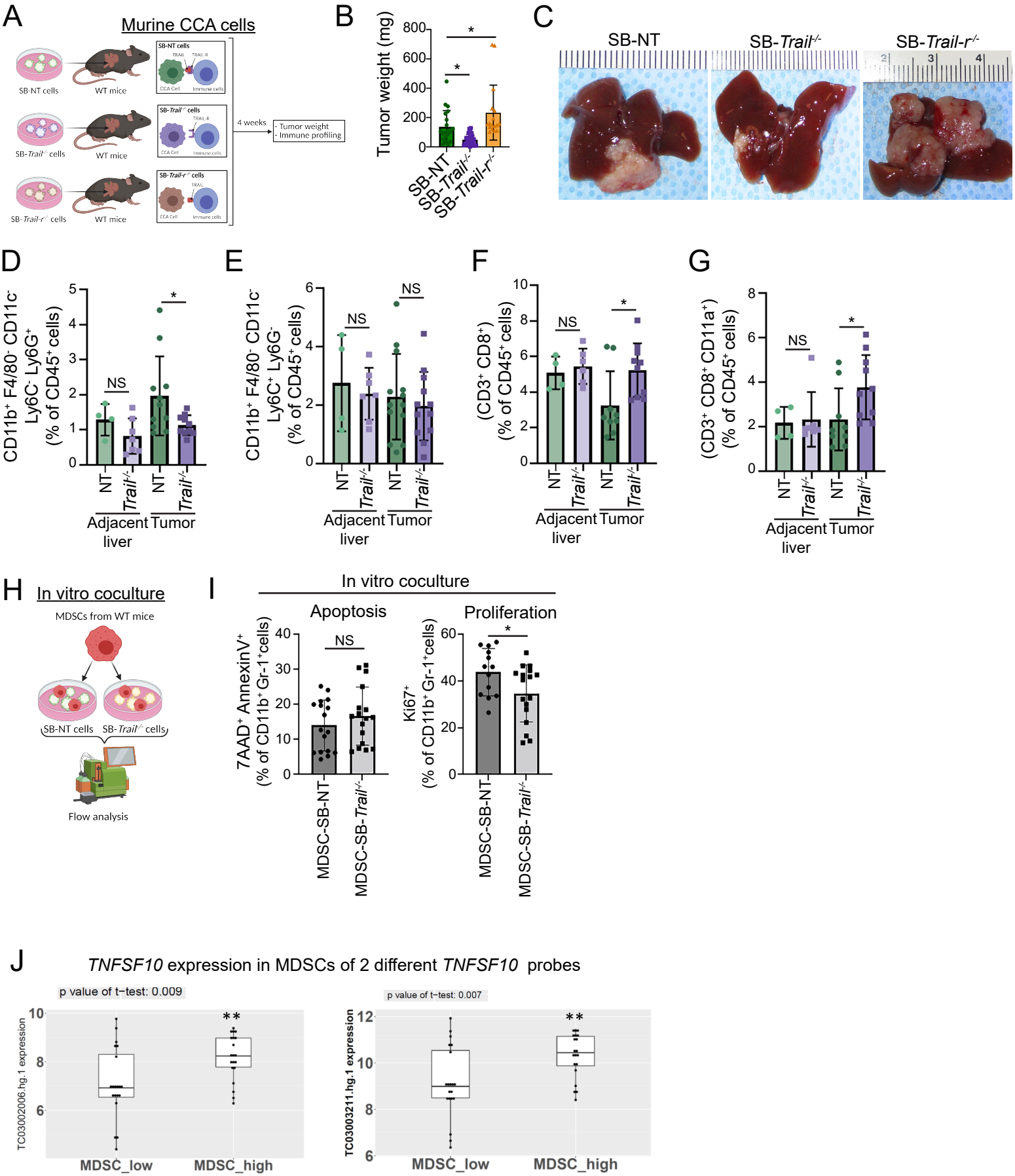
A
Murine CCA cells
SB-NT cells
WT mice
SB-Trail-/- cells
WT mice
SB-Trail-r-/- cells
WT mice
4 weeks
- Tumor weight
- Immune profiling
B
Tumor weight (mg)
SB-NT
SB-Trail-/-
SB-Trail-r-/-
C
SB-NT
SB-Trail-/-
SB-Trail-r-/-
D
CD11b+ F4/80- CD11c- Ly6C- Ly6G+ (% of CD45+ cells)
NS
*
NT
Trail-/-
Adjacent liver
Tumor
E
CD11b+ F4/80- CD11c- Ly6C+ Ly6G- (% of CD45+ cells)
NS
NS
F
(CD3+ CD8+) (% of CD45+ cells)
NS
*
G
(CD3+ CD8+ CD11a+) (% of CD45+ cells)
NS
*
H
In vitro coculture
MDSCs from WT mice
SB-NT cells
SB-Trail-/- cells
Flow analysis
I
In vitro coculture
Apoptosis
7AAD+ AnnexinV+ (% of CD11b+ Gr-1+cells)
NS
MDSC-SB-NT
MDSC-SB-Trail-/-
Proliferation
Ki67+ (% of CD11b+ Gr-1+cells)
*
J
TNFSF10 expression in MDSCs of 2 different TNFSF10 probes
p value of t-test: 0.009
TC03002006.hg.1 expression
**
MDSC_low
MDSC_high
p value of t-test: 0.007
TC03003211.hg.1 expression
**
MDSC_low
MDSC_high